Manipulating the frequency response of small high-frequency atomic force microscope cantilevers

IOP Publishing Journal Title
Journal **XX** (XXXX) XXXXXX https://doi.org/XXXX/XXXX

Manipulating the frequency response of small high-frequency atomic force microscope cantilevers

Harpreet Singh Brar[1] and Müjdat Balantekin[1,2]

[1] Previously affiliated with Electrical and Electronics Engineering, İzmir Institute of Technology, Turkey
[2] Electrical and Electronics Engineering, Gazi University, 06570 Ankara, Turkey
E-mail: harrpreetbrar@gmail.com, mujdatbalantekin@gazi.edu.tr

Received xxxxxx
Accepted for publication xxxxxx
Published xxxxxx

Abstract

We study small (less than 10 μm in length) high-frequency (greater than 1 MHz) cantilevers specially designed to be operated in high-speed atomic force microscopes for the visualization of biomolecular processes. The frequency responses of the first three flexural eigenmodes are investigated for the modified geometries. It is found that the *Q*-factors can be significantly altered in the desired way by reengineering the cantilever geometry without affecting its main operational parameters, such as the spring constant and the resonance frequency of the first flexural eigenmode, in the air environment. In addition, the higher-order flexural resonances can be moved away from the fundamental resonance with these geometrical modifications. The *Q*-factors in liquid, on the other hand, do not show a significant difference due to high viscous damping of the medium. Regular cantilevers modified by focused ion beam are used to demonstrate the validity of the finite element simulation model.

Keywords: atomic force microscopy, small high-frequency cantilever, flexural eigenmode, resonance frequency, *Q*-factor

1. Introduction

In life sciences, high-speed atomic force microscopy (HS-AFM) is now widely accepted as a dynamic event visualizer for numerous biological samples and processes, such as live cells, molecular machines, ATPases, proteins, enzymatic reactions, DNA-protein interactions, etc. [1-4]. HS-AFM's unique ability to observe surface topography of the samples with molecular resolution makes it a prominent tool in nanoscale measurements [5-7].

The cantilever is an indispensable and integral part of the HS-AFM. Cantilevers with a variety of shapes in different dimensions are now available with the advancement of the microfabrication technologies. The rectangular cantilevers are commonly employed in tapping-mode AFM experiments. These cantilevers typically have a length greater than 100 μm, a width greater than 20 μm, and a thickness greater than 1 μm. These dimensional constraints mainly arise from the limitations of the conventional AFM systems and their implications on the tip-sample interaction. The dimensions of the cantilever determine its spring constant and the resonance frequency. Therefore, an AFM system, which has a certain measurement bandwidth and laser spot size, can only utilize cantilevers that reside in an appropriate range of dimensions.

In an HS-AFM system, the cantilever size has to be minimized since this is the only way of obtaining high resonance frequency and low spring constant at the same time. The quality factor (*Q*-factor) of the cantilever is one other parameter that plays a vital role in the applied forces on the sample and the imaging speed. The *Q*-factor also depends on the cantilever dimensions and the operating environment by

means of various damping factors. In an HS-AFM imaging experiment, if the sample is scanned in air e.g., it may be desirable to have a *Q*-factor lower than the typically measured values to increase the speed at the expense of increased tip-sample forces, while it is desired to be higher than the typically measured values to increase the force sensitivity for biological specimens in liquid environment at the expense of decreased scan speed. Due to its strong influence on the operation of the AFM, the *Q*-control technique has been developed to improve the scan speed, but, this method requires additional electronics [8-11].

In the recently proposed fast actuation method [12,13], e.g., it is desired to have a low *Q*-factor for the fundamental eigenmode and high *Q*-factors for the higher eigenmodes. Also, an increased separation of fundamental and higher eigenmode resonances improves the quality of the acquired topography in this method. On the other hand, in a usual AFM experiment, it is better to suppress the higher eigenmodes to improve the image quality [14]. Furthermore, in multifrequency AFM [15-22] and mass sensing [23-25] applications, manipulating the frequency response of the cantilever could become useful.

The presented work concentrates on understanding the effects of geometrical modifications on the frequency response of small high-frequency AFM cantilevers in both air and liquid environments via finite element simulations. The target cantilever chosen in this study has been used in the state-of-the-art HS-AFM [4,26] to observe biomolecules at both high frame rates and low applied forces. The significances of these modifications and their possible implications on the HS-AFM operation are evaluated. This analysis allows us to reengineer the cantilever to alter the frequency response of it in the desired way.

2. Model

The cantilever probs the sample in air or liquid environments as shown in Fig. 1. The surrounding environment has a subtle influence on the resonance frequencies and *Q*-factors of the flexural eigenmodes of the cantilever. At an equilibrium pressure of 1 atm and temperature of 293 K, the density and dynamic viscosity are taken as 1.2 kg/m^3 and 18×10^{-6} Pa·s for air, and 1×10^3 kg/m^3 and 1×10^{-3} Pa·s for water, respectively.

The simulation model has to accurately take into account all the geometrical and physical features of the HS-AFM system. The cantilever deflection is assumed to be measured by the optical beam deflection technique, which puts a lower limit on the cantilever width. As seen in the figure, there is a gap (D_{TS}) between the free end of the cantilever and the sample surface, corresponding to the tip height. Also, an angle (θ) is present to assure that only the tip interacts with the sample.

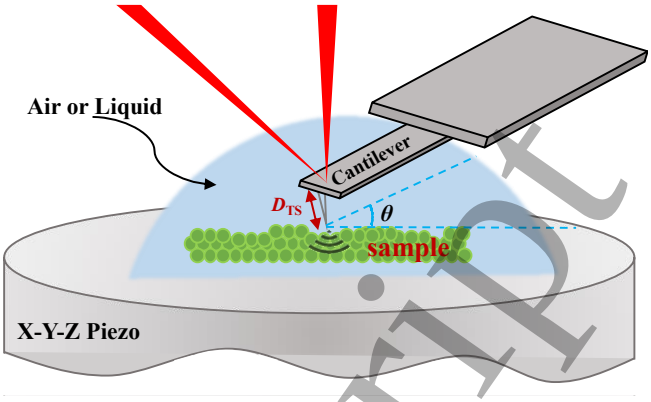

Figure 1. Close-up view of tip-sample interaction in a typical HS-AFM experiment.

In the simulated model (shown in Fg. 2), the cantilever beam and the substrate materials are chosen to be Silicon with Young's modulus of 170 GPa, Poisson's ratio of 0.28, and density of 2330 kg/m^3. The cantilever is fixed at one end, while the substrate is fixed on all sides. In the model, D_{TS} and θ are chosen to be 2 μm and 10°, respectively.

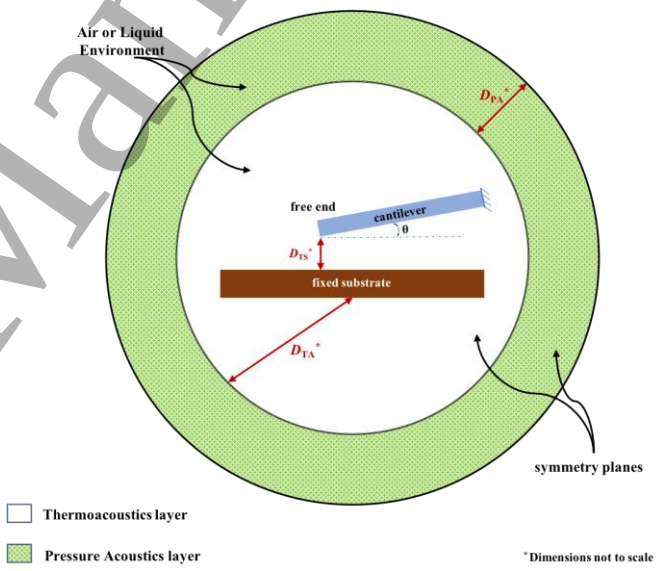

Figure 2. Model geometry.

When the cantilever beam operates in a vacuum environment, only intrinsic losses [27,28] $\boldsymbol{Q_{int}}^{-1}$ are in effect. Intrinsic losses may include coating loss [29] $\boldsymbol{Q_{coat}}^{-1}$ due to thin film coating on the cantilever, thermoelastic damping [30,31] $\boldsymbol{Q_{TED}}^{-1}$due to coupling of strain to temperature, anchor loss [32,33] $\boldsymbol{Q_{ankr}}^{-1}$due to diffusion of elastic waves into the support structure, and viscoelastic damping [34] $\boldsymbol{Q_{VED}}^{-1}$ due to loss modulus of cantilever material. If the cantilever is immersed in air or liquid, as in usual tapping-mode experiments, external losses $\boldsymbol{Q_{ext}}^{-1}$ becomes a dominant factor. The external losses consist of the squeeze

film effect [35-37] $\boldsymbol{Q_{sqz}}^{-1}$ due to a nearby surface, acoustic losses [38,39] $\boldsymbol{Q_{aco}}^{-1}$ due to acoustic waves generated by the vibrational motion of the cantilever, and viscous losses [40-48] $\boldsymbol{Q_{visc}}^{-1}$ due to viscous forces acting on the cantilever oscillating in the fluid. Therefore, the total loss $\boldsymbol{Q^{-1}}$ is obtained by

$$Q^{-1} = \underbrace{Q_{VED}{}^{-1} + Q_{ankr}{}^{-1} + Q_{coat}{}^{-1} + Q_{TED}{}^{-1}}_{\boldsymbol{Q_{int}}^{-1}} + \underbrace{Q_{sqz}{}^{-1} + Q_{aco}{}^{-1} + Q_{visc}{}^{-1}}_{\boldsymbol{Q_{ext}}^{-1}} \quad (1)$$

In this study, only the external damping factors are taken into account by assuming that the internal damping factors are negligible.

The cantilever and the substrate are both modeled as a linear elastic material in solid mechanics interface, and the surrounding fluid is modeled by using the thermoacoustics interface. The thermoacoustics interface solves the full linearized Navier-Stokes, energy and continuity equations for the propagation of compressible linear waves in a viscous fluid. The pressure acoustics layer is used for the propagation of acoustic waves and its outer boundary is terminated with spherical wave radiation condition. The radius of inner layer (D_{TA}) is about 5 times the length of the cantilevers under study, while the overall radius of the environment ($D_{TA} + D_{PA}$) is kept at 50 µm. The symmetry planes of the 3D simulation model are indicated in Fig. 2. The finite element analysis software package, COMSOL Multiphysics®, combines the aforementioned physics interfaces via multiphysics couplings, i.e., the acoustic-thermoacoustic and thermoacoustic-structure boundary couplings.

The eigenfrequency analysis was carried out to determine the resonance frequencies and the *Q*-factors for flexural eigenmodes. In this analysis, the real part of the computed eigenvalue is the damped resonance frequency and the imaginary part is related to the damping. We picked the highest *Q*-factor corresponding to the lowest imaginary part amongst the multiple computed results for each eigenmode.

3. Simulation Results

We first simulated a small rectangular beam with different dimensions. Here, the target cantilever is chosen to be the one used by Ando and co-workers in the state-of-the-art HS-AFM system [26] to visualize the biological molecules in physiological solutions. The fundamental eigenmode resonance frequencies in air and water, spring constant, and *Q*-factor in water for this 6-7 µm long, 2 µm wide, and 90 nm thick small rectangular cantilever (custom-made by Olympus) are specified to be 3.5 MHz, 1.2 MHz, 0.2 N/m, and ~2, respectively [49]. We compared three rectangular beams which have dimensions close to those of the target cantilever in air and liquid environments. A fair evaluation requires that both the spring constant and the resonance frequency of the fundamental eigenmode to be the same for all the cantilevers, because, these two parameters directly affect the scan speed and the forces applied to the sample. Since the cantilever dimensions have effects on these parameters as well as the *Q*-factors, the comparison of cantilevers that have different fundamental eigenmode spring constant and resonance frequency is not meaningful.

There are other constraints on the dimensions of the small cantilevers. First of all, the laser spot size in the state-of-the-art systems is about 1-2 µm. Additionally, the cantilever vibration amplitude is limited by the length of the beam. Therefore, there are going to be some lower bounds for the width and length of the beam, taken as 1.5 µm and 5 µm, respectively. The thickness, length, and width of each rectangular beam are selected such that the fundamental eigenmode resonance frequency in air (f_1) is 5 MHz (± 2%). These selections result in a spring constant (k) of 0.9 N/m (± 1%) and a resonance frequency of 1.5 MHz (± 2%) in liquid (f_{fl}).

The simulation results of the *Q*-factors for the first three flexural eigenmodes ($Q_{1\text{-}3}$) in air environment are listed in Table 1. The thickest cantilever with the lowest surface area has the highest *Q*-factors. As can be seen here, there is not enough room to play with the dimensions since the first and third rectangular beam ($\boldsymbol{C}_{\mathbf{RECT1}}$ and $\boldsymbol{C}_{\mathbf{RECT3}}$) dimensions have already reached to the lower bounds of the length and the width, respectively. In agreement with the analytically expected values, the ratio of the second to first (f_2/f_1) and third to first (f_3/f_1) flexural eigenmode resonance frequencies are found to be 6.3 and 17.8, respectively.

Table 1. The *Q*-factors for the first three flexural eigenmodes of small rectangular cantilevers in air environment.

Cantilever	Length (µm)	Width (µm)	Thickness (µm)	Q_1	Q_2	Q_3
C_{RECT1}	5.5	2.6	0.11	43	111	129
C_{RECT2}	6.0	2.0	0.13	49	118	140
C_{RECT3}	6.7	1.5	0.16	59	141	180

Next we studied the effects of basic modifications such as adding and removing a mass at both the fixed and the free ends of the cantilever. Figure 3 shows the locations of these holes and additional masses (Si) on the rectangular beam ($\boldsymbol{C}_{\mathbf{RECT3}}$). Here, $\boldsymbol{C}_{\mathbf{RECT3}}$ is chosen as the reference cantilever since it yields the maximum *Q*-factor amongst the three. The diameters of these holes and additional masses are 1 µm, and the thickness of the additional masses is equal to 0.16 µm, the original beam thickness.

The aim of adding a mass to the fixed end ($\boldsymbol{C}_{\mathbf{ADD\text{-}1\text{-}fixed}}$) is to increase the beam stiffness without significantly changing its

effective mass. Compared to C_{RECT3}, this results in higher *Q*-factors and resonance frequencies for all three flexural eigenmodes as expected. On the contrary, subtracting a mass on the same spot ($C_{SUBT\text{-}1\text{-}fixed}$) can be utilized to obtain the opposite effect. By adding a mass to the free end ($C_{ADD\text{-}1\text{-}free}$), on the other hand, it is aimed to increase the effective mass without significantly disturbing the beam stiffness. This simple modification results in higher *Q*-factors, but, lower resonance frequencies for all three flexural eigenmodes. Similarly, subtracting a mass on the same location ($C_{SUBT\text{-}1\text{-}free}$) causes the opposite effect. The exceptions to these results are f_3 of $C_{SUBT\text{-}1\text{-}free}$ and Q_2 of $C_{SUBT\text{-}1\text{-}fixed}$ and $C_{SUBT\text{-}1\text{-}free}$.

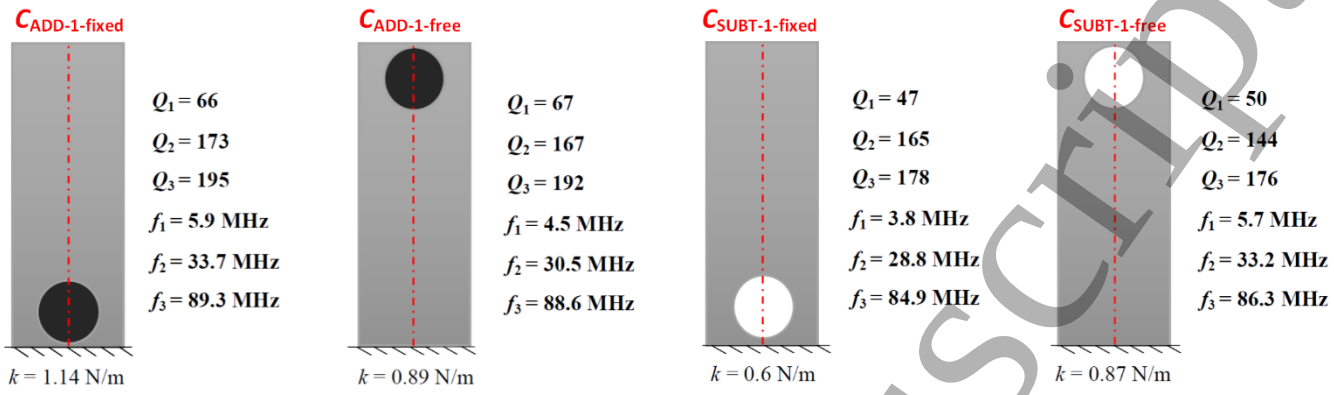

Figure 3. Changing the *Q*-factors via simple addition and subtraction of masses from fixed and free ends of the rectangular cantilever. Adding a mass to the fixed ($C_{ADD\text{-}1\text{-}fixed}$) and free ($C_{ADD\text{-}1\text{-}free}$) ends. Subtracting a mass from the fixed ($C_{SUBT\text{-}1\text{-}fixed}$) and free ($C_{SUBT\text{-}1\text{-}free}$) ends. The vertical lines indicate the center of the beam and the location of the symmetry plane.

Once the significance of simple addition and removal of material from certain locations of the beam was understood, we concentrated on the combinations of these modifications. These include both addition and removal of material at different spots on the rectangular beam. Figure 4 presents the simulation results in air just for four of them. In this figure, $C_{ADD\text{-}5}$ is the one on which there are 5 equally distanced added masses which have the same thickness and diameter of the mass on $C_{ADD\text{-}1\text{-}fixed}$. Likewise, $C_{SUBT\text{-}5}$ is obtained by opening 5 holes on the same spots. Here, the changes in the *Q*-factors are more pronounced and in the expected directions, but, the deviations from the reference spring constant are higher.

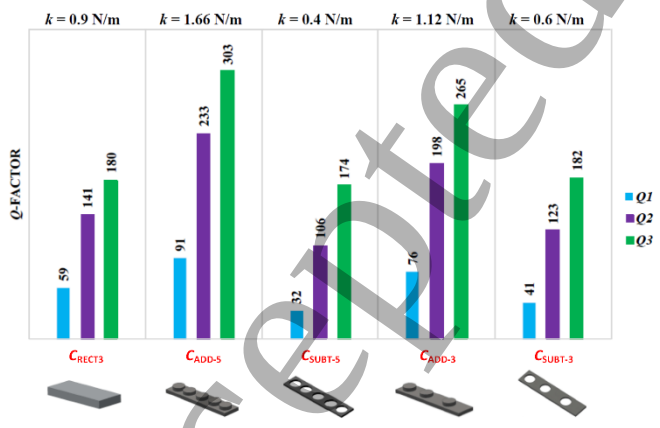

Figure 4. Comparison of the *Q*-factors of the first three flexural eigenmodes of the modified cantilevers with the ones obtained for the original rectangular beam (C_{RECT3}).

The effects of adding and removing material on the special positions, such as high-amplitude locations of the third flexural eigenmode shape of the original rectangular beam ($C_{ADD\text{-}3}$ and $C_{SUBT\text{-}3}$), were also investigated. The change in the *Q*-factors for $C_{ADD\text{-}3}$ are less distinct compared to $C_{ADD\text{-}5}$, but, the spring constant is closer to the reference value. There is a similar situation between $C_{SUBT\text{-}3}$ and $C_{SUBT\text{-}5}$ as well. f_2/f_1 and f_3/f_1 do not deviate much from the original value for $C_{ADD\text{-}5}$ and $C_{SUBT\text{-}5}$, but, they are found to be 6.0 ($C_{SUBT\text{-}3}$) and 6.6 ($C_{ADD\text{-}3}$); 16.3 ($C_{SUBT\text{-}3}$) and 19.8 ($C_{ADD\text{-}3}$), respectively.

To increase the variation in the *Q*-factors further, advanced approaches have to be resorted, such as reshaping the original rectangular beam. In Fig. 5, we see two examples of reshaped cantilevers in order to increase ($C_{INC\text{-}Q}$) and decrease ($C_{DEC\text{-}Q}$) the *Q*-factor. In the design of $C_{INC\text{-}Q}$, we aimed to increase the mass at the free end of the cantilever, the mass in the mid section of the beam and the surface area are minimized, while the fixed end thickness is adjusted to keep the stiffness close to the reference level. In this design, the fixed and free ends are square in shape with a side length of 1.5 µm (the width of C_{RECT3}), while the mid connecting region is 3.7 µm in length and only 50 nm in width. Here, the lowest possible width is assumed to be limited by the fabrication technology. The thickness is uniform throughout the cantilever and it is chosen to be 0.55 µm. The fundamental eigenmode *Q*-factor of $C_{INC\text{-}Q}$ is seen to be more than double of that of the reference cantilever, although their spring constants are close to each other.

The design of $\boldsymbol{C}_{\text{DEC-Q}}$, on the other hand, was done to minimize the *Q*-factor as much as possible by decreasing both the stiffness and the effective mass of the cantilever. The design assumes that the starting cantilever is again $\boldsymbol{C}_{\text{RECT3}}$. It can be thinned down to 0.1 µm first, and then the unwanted portions can be etched away leaving a square-shaped free end with a side length of 1.5 µm (approximately the laser spot size) and a 50 nm wide lever. This design results in the lowest *Q*-factor amongst the others. Although the resonance frequency is reduced down to 1.2 MHz in air, a substantial reduction in the *Q*-factor can enable this much softer cantilever (0.012 N/m) to be used in high-speed imaging. Interestingly, for both cantilevers, we observed that f_2/f_1 is much larger than that of the original rectangular beam. Moreover, the third flexural eigenmode was not observed for these cantilevers due to clamped-clamped like beam behavior, i.e., the displacement of the free end is almost zero.

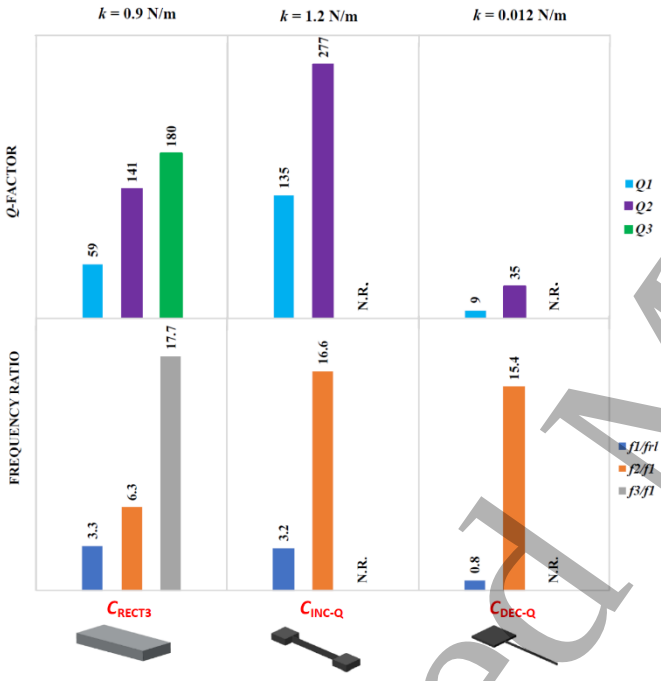

Figure 5. Reshaping the rectangular cantilever (C_{RECT3}) to increase ($\boldsymbol{C}_{\text{INC-Q}}$) and decrease ($\boldsymbol{C}_{\text{DEC-Q}}$) the *Q*-factor. f_{rl} = 1.5 MHz. N.R.: No Result.

4. Experimental Validation

The model verification needs to be done by measuring the *Q*-factors and resonance frequencies of the modified small cantilevers. Since the AFM systems that we use have a laser spot size of about 30 µm and a measurement bandwidth of approximately 2 MHz, not suitable for small high-frequency cantilevers, we used regular cantilevers to validate our model. The test cantilever (Aspire CFMR, Nanoscience Instruments) that we use has a length of 225 µm, a width of 42 µm, and a thickness of 3µm. The nominal spring constant and the resonance frequency values are specified by the manufacturer as 3 N/m and 75 kHz, respectively. The SEM micrograph of the reference test cantilever ($\boldsymbol{TC}_{\text{REF}}$) is seen in Fig. 6.

The SEM micrographs of the focused ion beam (FIB, FEI Nanolab 600i) modified test cantilevers to increase the *Q*-factor ($\boldsymbol{TC}_{\text{INC-Q}}$) and to decrease the *Q*-factor ($\boldsymbol{TC}_{\text{DEC-Q}}$) are also seen in the same figure. The modifications were done such that the test cantilevers resemble the ones seen in Fig. 5. The test cantilever was first reshaped and then approximately 3 µm Platinum was deposited on the cantilever to obtain the final shape of $\boldsymbol{TC}_{\text{INC-Q}}$ that has an approximately 6 µm uniform thickness. The free and the fixed ends can be identified by two square regions with an area of ≈ 40 µm × 40 µm, while the mid interconnect in between has a width of 4 um. $\boldsymbol{TC}_{\text{DEC-Q}}$ was obtained by again first reshaping the original beam, and in addition, only the free end (with an area of ≈ 40 µm × 40 µm) thickness was reduced down to ≈ 0.5 µm, while the rest of the cantilever has a width and a thickness of about 4 um and 3 um, respectively.

The resonance frequencies and *Q*-factors for the first two flexural eigenmodes of all three cantilevers are measured in air before (with Bruker Multimode 8) and after (with Asylum Research MFP-3D) the FIB manipulation. The measurement results along with the expected simulation results are summarized in Table 2. In this case, the simulations were done without the substrate to comply with the experiments.

5. Discussion

A cantilever having both low spring constant and high resonance frequency, as desired in high-speed biomolecular imaging, requires that $\sqrt{km^*}$ has to be reduced, where m^* is the effective mass of the cantilever. Since the *Q*-factor is proportional to $\sqrt{km^*}$, this requirement naturally results in a low *Q*-factor for smaller beams. Rectangular beams with uniform thicknesses are widely used due to easy fabrication process and simple analytical relation between its spring constant and dimensions. However, the desired spring constant and the resonance frequency may not be achievable at the same time with small rectangular beams. $f_1 \propto t/l^2$ for a rectangular beam not loaded by the fluid, and $k \propto wt^3/l^3$, where *t*, *l*, and *w* are the thickness, length, and width of the beam, respectively. If f_1 is to be increased by increasing *t* or decreasing *l*, *w* needs to be decreased such that *k* remains unchanged. However, this may not be feasible due to system limitations.

Material added to or subtracted from specific spots can manipulate the *Q*-factor in a limited range, but, this approach can be more effective than changing the dimensions of the rectangular beam. As a comparison, we increased the thickness of $\boldsymbol{C}_{\text{RECT3}}$ to 0.2 µm, which yielded a higher *k* but a lower Q_1 than those of $\boldsymbol{C}_{\text{ADD-5}}$. This 0.2 µm-thick cantilever is further studied to determine the dominant external loss factor. The dynamic viscosity of the air is decreased by thousandfold to bring down the viscous damping to a negligible level. Under

this condition, Q_1 is increased from 85 to 9×10^3 (no internal damping), which means that the viscous damping is the dominant loss component. The quality factor for the *n*th mode of rectangular beam vibration Q_n due to viscous damping derived by Sader is given as [50]

$$Q_n = \frac{(4\rho_c t/\pi\rho w)+\Gamma_r(\omega_{R,n})}{\Gamma_i(\omega_{R,n})}, \quad (2)$$

where, ρ_c and ρ are the densities of the cantilever and the fluid, respectively. The real (r) and the imaginary (i) parts of the hydrodynamic function Γ for the nth flexural eigenmode resonance frequency ($\omega_{R,n}$) are derived analytically [51] and for $1 \le \beta \le 1\times10^3$ approximated to [42]

$$\Gamma_r \cong 1.1 + 3.8\,\delta/w$$
$$\Gamma_i \cong 3.8\,\delta/w + 2.7(\delta/w)^2, \quad (3)$$

where $\beta = w^2/2\delta^2$ is the normalized Reynolds number as defined in [50], $\delta = \sqrt{2\eta/\rho\omega}$ is the viscous layer thickness, and η is the fluid viscosity. At room temperature and atmospheric pressure, the Knudsen number is 0.05 for w = 1.5 µm. Therefore the continuum model can be considered fairly accurate here [39,43]. Note also that the continuum model can still be applicable for $\boldsymbol{C}_{\mathbf{INC\text{-}Q}}$ and $\boldsymbol{C}_{\mathbf{DEC\text{-}Q}}$ since δ is higher than the molecular mean free path [39]. By using equations (2) and (3), and f_1 = 6.3 MHz, Q_1 is obtained to be 106, which also indicates that the viscous damping surpasses the other external loss factors.

On the other hand, Q_2 and Q_3 are predicted by equations (2) and (3) to be 325 and 584, while the simulations yielded 207 and 329, respectively. If η is decreased by thousandfold, Q_2 and Q_3 are obtained from simulations as 3.7×10^3 and 398, respectively. This result tells us that at the second eigenmode (40 MHz) the viscous damping is still dominant, but, at the third eigenmode (115 MHz) the acoustic damping is now the prominent loss component. At 115 MHz the acoustic wavelength λ_a in air is 3 µm, while the flexural wavelength λ_f of the third eigenmode is about 5.4 µm. Since the radiation efficiency increases as λ_a becomes comparable to λ_f and w, and it is inversely proportional to the Q-factor [38,39], the acoustic radiation limits the Q-factor at this frequency. Moreover, the effect of squeeze film damping was also studied for this cantilever by just removing the substrate, and its effect was found to be less than 10%.

The analysis was not only done in air but in water as well. For $\boldsymbol{C}_{\mathbf{RECT3}}$, Q_1, Q_2, and Q_3 are found to be 1.7, 4.2, and 7, respectively. Q_1 could be as low as 0.3 for $\boldsymbol{C}_{\mathbf{DEC\text{-}Q}}$ and as high as 1.8 for both $\boldsymbol{C}_{\mathbf{ADD\text{-}5}}$ and $\boldsymbol{C}_{\mathbf{INC\text{-}Q}}$ due to high viscous damping of the water. f_2/f_1 and f_3/f_1 are found to be about 8 and 26 for $\boldsymbol{C}_{\mathbf{RECT3}}$, and they are slightly increasing in the order of $\boldsymbol{C}_{\mathbf{RECT3}}\rightarrow\boldsymbol{C}_{\mathbf{RECT2}}\rightarrow\boldsymbol{C}_{\mathbf{RECT1}}$. The higher f_2/f_1 and f_3/f_1 values in water are the results of smaller mass loading effect on the higher eigenmodes. On the other hand, f_2/f_1 is found to be much higher, approximately 19 and 43 for $\boldsymbol{C}_{\mathbf{INC\text{-}Q}}$ and $\boldsymbol{C}_{\mathbf{DEC\text{-}Q}}$, respectively, while the third flexural eigenmode was not observed for these cantilevers as in air environment.

The test cantilevers showed the same tendency of $\boldsymbol{C}_{\mathbf{INC\text{-}Q}}$ and $\boldsymbol{C}_{\mathbf{DEC\text{-}Q}}$ in terms of Q-factors. On the other hand, there is a substantial difference between the experimentally and numerically obtained second eigenmode resonance frequency of the modified cantilevers. This difference cannot be easily interpreted with mismatched thickness or material property (for $\boldsymbol{TC}_{\mathbf{INC\text{-}Q}}$) of the cantilevers used in the experiments since Q_1 and Q_2 of both $\boldsymbol{TC}_{\mathbf{INC\text{-}Q}}$ and $\boldsymbol{TC}_{\mathbf{DEC\text{-}Q}}$ show deviation from the simulations in the opposite directions. But, the discrepancy in the measured Q-factors could partly be attributed to the imperfect mechanical coupling between the dither piezo and the cantilever substrate [52] since there is a considerable difference even in the before and after measurement of Q_2 of the unmodified test cantilever.

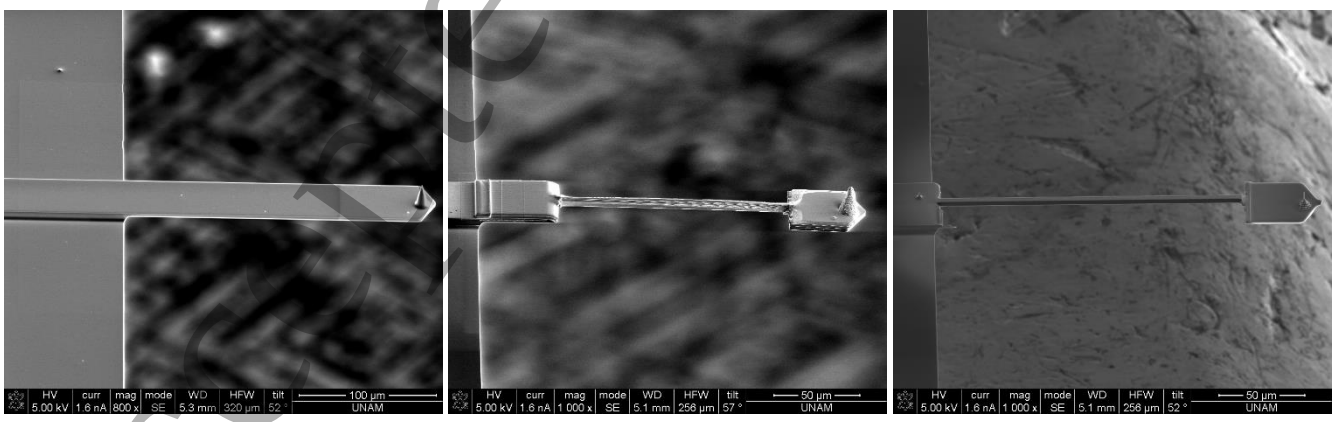

Figure 6. SEM micrographs of the FIB modified regular test cantilevers. (Left) Reference test cantilever ($\boldsymbol{TC}_{\mathbf{REF}}$), (Middle) modified test cantilever to increase the Q-factor ($\boldsymbol{TC}_{\mathbf{INC\text{-}Q}}$), (Right) modified test cantilever to decrease the Q-factor ($\boldsymbol{TC}_{\mathbf{DEC\text{-}Q}}$).

Table 2. *Q*-factor and resonance frequency measurement results for the first and second flexural eigenmodes of the test cantilevers before and after the manipulation along with expected simulation results.

Cantilever	BEFORE THE MANIPULATION				AFTER THE MANIPULATION				SIMULATION			
	f_1 (kHz)	f_2 (kHz)	Q_1	Q_2	f_1 (kHz)	f_2 (kHz)	Q_1	Q_2	f_1 (kHz)	f_2 (kHz)	Q_1	Q_2
TC_{REF}	74	469	184	626	74	469	194	538	82	517	229	621
$TC_{INC\text{-}Q}$	74	462	239	557	62	536	495	669	85	1040	391	1042
$TC_{DEC\text{-}Q}$	75	479	195	604	61	395	89	155	67	776	40	223

6. Conclusion

We studied small high-frequency cantilevers as they greatly influence the dynamics of the HS-AFM which becomes more and more prominent in the live imaging of biomolecules. The geometric modifications prove useful to adjust the *Q*-factor in air environment. In water, we did not obtain significant variance in the *Q*-factors due to high viscous damping. The ratio of the second eigenmode resonance to the fundamental one is greatly increased for reshaped cantilevers which makes them preferable in the actuatorless HS-AFM imaging [12,13]. If the original cantilever is in rectangular shape, it is difficult to lower the *Q*-factor further for high-speed imaging in air since there is not enough material left to remove. By utilizing the outcomes of the basic modifications, customized arbitrary geometries could be complemented by judiciously selected cantilever materials to push the scan rate or sensitivity to the extremes for a specific HS-AFM, multifrequency, or mass sensing application in air or liquid.

Acknowledgements

This work was supported by TÜBİTAK (Grant No. 117F186). The authors would like to thank Mustafa Güler (Bilkent University, UNAM) for FIB modifications, Semih Bozkurt (Bilkent University, UNAM) and Mine Bahçeci (İzmir Institute of Technology, Center for Materials Research) for AFM measurements. We also acknowledge the genuine support of Prof. Yusuf Baran, the Rector of İzmir Institute of Technology.

References

[1] Uchihashi T, Lino R, Ando T and Noji H 2011 *Science* **333** 755
[2] Kodera N, Yamamoto D, Ishikawa R and Ando T 2010 *Nature* **468** 72
[3] Ando T 2013 *FEBS Lett.* **587** 997
[4] Rajendran A, Endo M and Sugiyama H 2014 *Chem. Rev.* **114** 1493
[5] Ando T 2014 *Curr. Opin. Struct. Biol.* **28** 63
[6] Ando T, Uchihashi T and Scheuring S 2014 *Chem. Rev.* **114** 3120
[7] Eghiaian F, Rico F, Colom A, Casuso I and Scheuring S 2014 *FEBS Lett.* **588** 3631
[8] Sulchek T *et al* 2000 *Appl. Phys. Lett.* **76** 1473
[9] Antognozzi M, Szczelkun M D, Humphris A D L and Miles M J 2003 *Appl. Phys. Lett.* **82** 2761
[10] Kodera N, Yamashita H and Ando T 2005 *Rev. Sci. Instrum.* **76** 053708
[11] Balantekin M and Degertekin F L 2011 *Ultramicroscopy* **111** 1388
[12] Balantekin M, Satir S, Torello D and Degertekin F L 2014 *Rev. Sci. Instrum.* **85** 123705
[13] Balantekin M 2015 *Ultramicroscopy* **149** 45
[14] Karvinen K S and Moheimani S O R 2014 *Ultramicroscopy* **137** 66
[15] Lazano J R and Garcia R 2008 *Phys. Rev. Lett.* **100** 076102
[16] Jesse S, Kalinin S V, Proksch R, Baddorf A P and Rodriguez B J 2007 *Nanotechnology* **18** 435503
[17] Garcia R and Herruzo E T 2012 *Nature Nanotech.* **7** 217
[18] Ebeling D and Solares S D 2013 *Beilstein J. Nanotechnol.* **4** 198
[19] Dietz C, Schulze M, Voss A, Riesch C and Stark R W 2015 *Nanoscale* **7** 1849
[20] Ruppert M G and Moheimani S O R 2016 *IEEE Trans. Control Syst. Technol.* **24** 1149
[21] Loganathan M and Bristow D A 2014 *Rev. Sci. Instrum.* **85** 043703
[22] Baumann M and Stark R W 2010 *Ultramicroscopy* **110** 578
[23] Dohn S, Sandberg R, Svendsen W and Boisen A 2005 *Appl. Phys. Lett.* **86** 233501
[24] Tamayo J *et al* 2013 *Chem. Soc. Rev.* **42** 1287
[25] Li M, Tang H X and Roukes M L 2007 *Nature Nanotech.* **2** 114
[26] Ando T 2012 *Nanotechnology* **23** 062001
[27] Lübbe J *et al* 2010 *Meas. Sci. Technol.* **21** 125501
[28] Yasumura K Y *et al* 2000 *J. Microelectromech. Syst.* **9** 117
[29] Sandberg R, Molhave K, Boisen A and Svendsen W 2005 *J. Micromech. Microeng.* **15** 2249
[30] Lifshitz R and Roukes M L 2000 *Phys. Rev. B* **61** 5600
[31] Candler R N *et al* 2006 *J. Microelectromech. Syst.* **15** 927
[32] Hao Z, Erbil A and Ayazi F 2003 *Sens. Actuators A* **109** 156
[33] Judge J A *et al* 2007 *J. Appl. Phys.* **101** 013521
[34] Adams J D *et al* 2015 *Nature Nanotech.* **11** 147
[35] Bao M and Yang H 2007 *Sens. Actuators A* **136** 3
[36] Green C P and Sader J E 2005 *J. Appl. Phys.* **98** 114913
[37] Tung R C, Jana A and Raman A 2008 *J. Appl. Phys.* **104** 114905

[38] Lochon F, Dufour I and Rebiere D 2006 *Sens. Actuators B* **118** 292
[39] Judge J A, Vignola J F and Jarzynski J 2008 *Appl. Phys. Lett.* **92** 124102
[40] Blom F R, Bouwstra S, Elwenspoek M and Fluitman J H J 1992 *J. Vac. Sci. Technol. B* **10** 19
[41] Vignola J F *et al* 2006 *Appl. Phys. Lett.* **88** 041921
[42] Maali A *et al* 2005 *J. Appl. Phys.* **97** 074907
[43] Bhiladvala R B and Wang Z J 2004 *Phys. Rev. E* **69** 036307
[44] Lübbe J *et al* 2011 *Meas. Sci. Technol.* **22** 055501
[45] Basak S, Raman A and Garimella S V 2006 *J. Appl. Phys.* **99** 114906
[46] Van Eysden C A and Sader J E 2007 *J. Appl. Phys.* **101** 044908
[47] Lee J H *et al* 2007 *J. Micromech. Microeng.* **17** 139
[48] Kirstein S, Mertesdorf M and Schönhoff M 1998 *J. Appl. Phys.* **84** 1782
[49] Uchihashi T, Kodera N and Ando T 2012 *Nat. Protoc.* **7** 1193
[50] Sader J E 1998 *J. Appl. Phys.* **84** 64
[51] Van Eysden C A and Sader J E 2006 *Phys. Fluids* **18** 123102
[52] Jensen J and Hegner M 2012 *J. Sensors* **2012** 258381